Crystallization Kinetics and Crystalline Morphology of Poly(ethylene naphthalate) and Poly(ethylene terephthalate-*co*-bibenzoate)

Y. S. Hu,[1] M. Rogunova,[1] D. A. Schiraldi,[2] A. Hiltner,[1] E. Baer[1]

[1] *Department of Macromolecular Science and Center for Applied Polymer Science, Case Western Reserve University, Cleveland, Ohio 44106-7202*
[2] *KoSa, 1551 Sha Lane, Spartanburg, South Carolina 29304*

Received 3 December 2001; accepted 15 January 2002

ABSTRACT: Copolymers of ethylene glycol with 4,4′-bibenzoic acid and terephthalic acid are known to crystallize rapidly to surprisingly high levels of crystallinity. To understand this unusual behavior, the isothermal crystallization of poly(ethylene bibenzoate-*co*-terephthalate) in the molar ratio 55:45 (PETBB55) was studied. Poly(ethylene naphthalate) (PEN) was included in the study for comparison. The kinetics of isothermal crystallization from the melt and from the amorphous glass was determined using differential thermal analysis. The results were correlated with the crystalline morphology as observed with atomic force microscopy (AFM). Crystallization of PEN exhibited similar kinetics and spherulitic morphology regardless of whether it was cooled from the melt or heated from the glass to the crystallization temperature. The Avrami coefficient was close to 3 for heterogeneous nucleation with 3-dimensional crystal growth. The copolymer PETBB55 crystallized much faster than did PEN and demonstrated different crystallization habits from the melt and from the glass. From the melt, PETBB55 crystallized in the "normal" way with spherulitic growth and an Avrami coefficient of 3. However, crystallization from the glass produced a granular crystalline morphology with an Avrami coefficient of 2. A quasi-ordered melt state, close to liquid crystalline but lacking the order of a recognizable mesophase, was proposed to explain the unusual crystallization characteristics of PETBB55. © 2002 Wiley Periodicals, Inc. J Appl Polym Sci 86: 98–115, 2002

Key words: polyesters; crystallization; morphology; spherulites

INTRODUCTION

Copolymerization with 4,4′-bibenzoic acid enhances the oxygen barrier of poly(ethylene terephthalate) (PET) when oriented[1] and imparts a higher modulus, strength, and temperature stability to the PET fiber.[2] The homopolymer poly(ethylene 4,4′-bibenzoate) (PEBB) has been reported to be liquid crystalline[3,4]; however, it melts close to its decomposition temperature, so the mesophase has not been characterized. Polyesters of 4,4′-bibenzoic acid with higher aliphatic diols are more tractable and these form a highly ordered thermotropic smectic phase.[3–7] Liquid crystalline polymers (LCPs) characteristically exhibit an outstanding gas barrier and exceptional fiber properties. It may be that the copolymers of 4,4′-bibenzoic acid are "frustrated" LCPs.[8,9] The possibility that they take on liquid-crystalline characteristics when oriented from the disordered glass or melt would explain the observed property enhancements.

The recent development of a potentially low-cost process for the monomer may spur interest in the attractive properties of 4,4′-bibenzoic acid polymers and copolymers.[10] Copolymers of ethylene glycol with terephthalic acid and 4,4′-bibenzoic acid have glass transition temperatures intermediate between those of PET and poly(ethylene naphthalate) (PEN).[11] Surprisingly, PET modified with 4,4′-biphenyl-containing comonomers crystallizes rapidly, indeed more rapidly than do PET and PEN, to a high level of crystallinity.[12,13] Copolymers of ethylene glycol with 4,4′-bibenzoic acid and 2,6-naphthoic acid also crystallize readily with a uniform comonomer inclusion when the concentration of naphthalate is high.[14] Despite this unusual characteristic (indeed, copolymerization is often used to retard the crystallization of PET), the crystallization kinetics and crystalline morphology of 4,4′-bibenzoic acid copolymers have not been described.

In contrast, the extensive literature on the crystallization of PET was the subject of a recent review,[15] and crystallization of PEN has also been studied.[16,17] These polymers crystallize from the melt or from the quenched amorphous glass if it is heated above the glass transition (cold crystallization). In both cases, the

Correspondence to: A. Hiltner.
Contract grant sponsor: KoSa.
Contract grant sponsor: National Science Foundation; contract grant numbers: DMR 9975774; DMR 9986467.

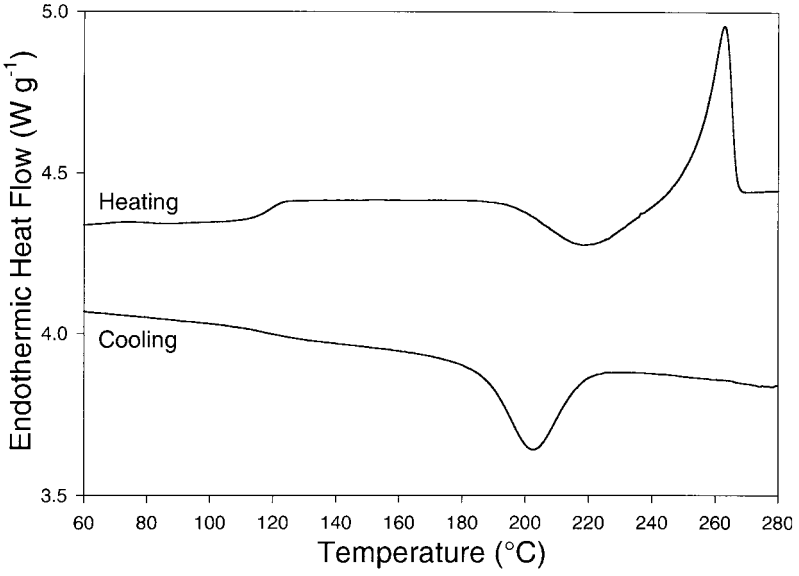

Figure 1 Heating and cooling thermograms of quenched PEN film obtained with a scanning rate of 10°C min^{-1}.

time dependence for the isothermal development of crystallinity is described by the Avrami equation. Although reported values of the exponent n range from 2 to 4, $n = 2.5$ is a good representative value for both PET and PEN. The dominant morphology is spherulitic. However, hedritelike structures sometimes grow at higher temperatures.

A copolymer of ethylene glycol with 4,4′-bibenzoic acid and terephthalic acid in the molar ratio 55:45 (PETBB55) was chosen for this investigation. In undertaking the study, the crystallization of PEN under the same conditions was examined also for purposes of comparison. The kinetics of isothermal crystallization from the melt and from the amorphous glass is correlated with the crystalline morphology as observed with atomic force microscopy (AFM).

EXPERIMENTAL

Materials

PEN and PETBB55 were provided by KoSa (Spartanburg, SC) in the form of extruded pellets. The chemical structures of the polyesters are

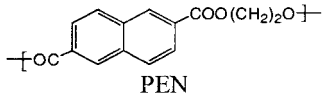

PEN

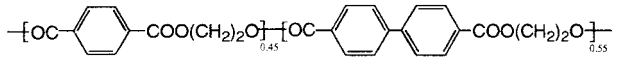

PETBB55

The pellets were dried in a vacuum and 0.3-mm-thick films were compression-molded at 310°C and quenched in cold water. The clear films were used in the kinetic studies and to prepare specimens for X-ray diffraction and AFM.

Isothermal crystallization

Isothermal crystallization was carried out in a Perkin–Elmer DSC7 calibrated with indium and tin standards. All tests were performed in a nitrogen atmosphere. Specimens were dried overnight at ambient temperature in a vacuum. The specimen weight was about 6 mg; the actual weight was determined with ± 2-μg precision. Specimens were enclosed in aluminum pans; the reference aluminum pan contained the appropriate number of extra lids needed to balance the heat capacity and achieve the best baseline.

For melt crystallization of PEN, specimens were melted at 290°C for 3 min and rapidly cooled to the crystallization temperature at 100°C min^{-1}. For cold crystallization, specimens were heated at 100°C min^{-1} to the crystallization temperature. Isothermal crystallization was performed at 180, 190, 200, 210, 220, and 230°C. Isothermal crystallization of PETBB55 was conducted in the same way except that the melt crystallization temperatures were 213, 215, 217, and 219°C and the cold-crystallization temperatures were 109, 110, and 111°C. Melt crystallization of PEN was also performed at 220°C after specimens were melted at either 300 or 310°C for 3 min. A new specimen was used for each isothermal test.

The determination of time $t = 0$ for the kinetic analysis merits discussion. The assumption that no crystallization occurs before the specimen reaches the crystallization temperature is usually acceptable because the onset of crystallization usually requires an induction period. This assumption becomes less tena-

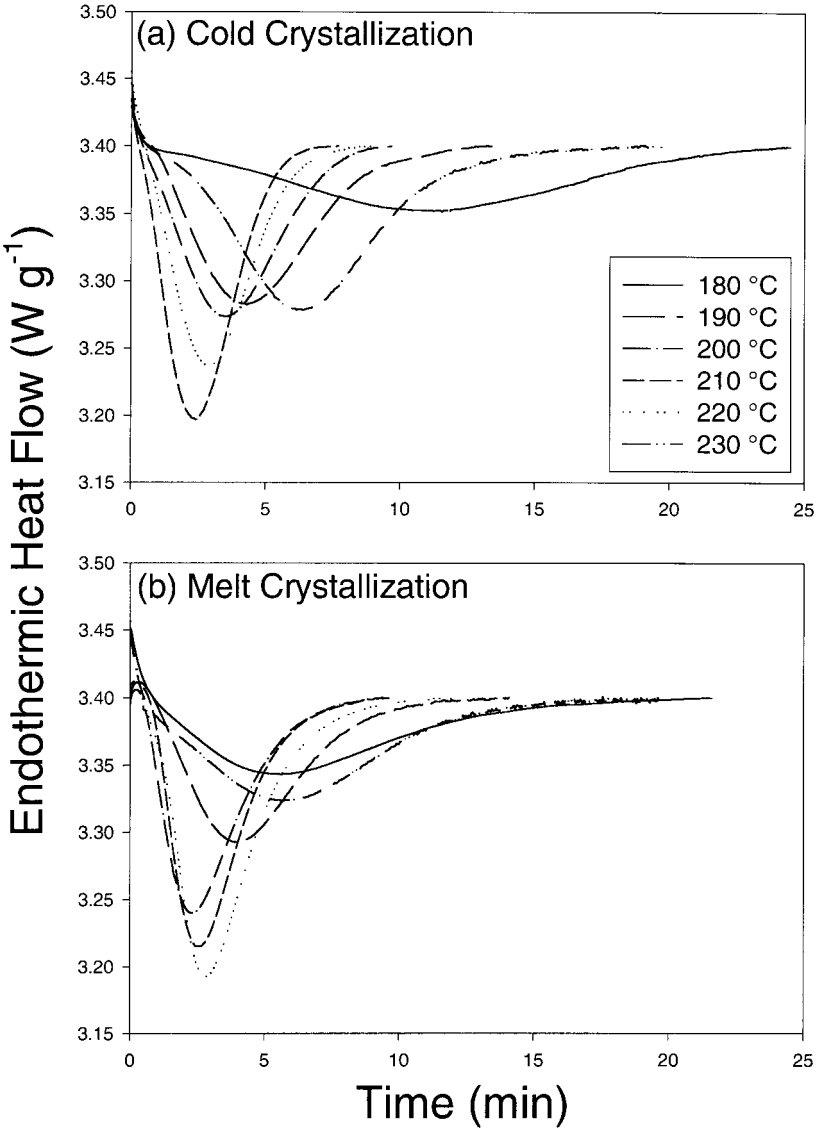

Figure 2 Isothermal DSC traces for crystallization of PEN: (a) cold-crystallized at the temperature indicated; (b) melted at 290°C and crystallized at the temperature indicated.

ble as the isothermal crystallization rate increases.[18] Therefore, a procedure was developed for minimizing the time required to achieve a stable instrumental baseline. By optimizing the number of lids in the reference pan, it was usually possible to reach a stable isothermal baseline in 0.3 min. The time t for the kinetic analysis was taken as the elapsed time minus 0.3 min.

X-ray diffraction

Specimens were compression-molded for wide-angle X-ray scattering (WAXS). Melt-crystallized films were transferred directly from the compression molder to an oven at the desired crystallization temperature. Cold-crystallized films were quenched and crystallized in the oven. X-ray diffraction was performed at room temperature in a Philips diffractometer with CuKα_1 radiation and a slit angle of 0.5°.

AFM

Based on the kinetic studies, various time points were chosen to arrest crystallization and examine the morphology. Specimens were isothermally crystallized in the DSC and quenched by cooling at nominally 300°C min^{-1}.

Specimens were sectioned with an Ultramicrotome (MT6000-XL from RMC, Tucson, AZ) and etched. Cold- and melt-crystallized PEN and melt-crystallized PETBB55 were etched following the method of Shabana et al.[19] This method was also used to etch PETBB55 that was quenched in the DSC directly from the melt without isothermal crystallization. The poly-

mer was etched for 30–60 min in a potassium permanganate solution at ambient temperature. The solution contained 10 mg of potassium permanganate per milliliter of a 10:4:3 vol:vol:vol mixture of concentrated sulfuric acid, orthophosphoric acid (85%), and water.

Cold-crystallized PETBB55 and uncrystallized, compression-molded films of PETBB55 and PEN were etched more gently using the procedures of Organ et al.[20] and Hudson et al.[21]The polymer was etched for 30–60 min in a 40 wt % aqueous methylamine solution at 40°C. Etching removed the amorphous phase to a depth of about 20–40 nm to expose the interior crystalline structure.

The etched surfaces were examined by AFM; the images were obtained in air at ambient conditions using a Nanoscope IIIa MultiMode head from Digital Instruments (Santa Barbara, CA). Experiments were conducted in the tapping mode using Si probes with 50 N m^{-1} spring constant and resonance frequencies in the range 284–362 kHz. The tip had a radius of 10 nm. Height and phase images were recorded simultaneously.

RESULTS AND DISCUSSION

Isothermal crystallization kinetics of PEN

The heating thermogram of the compression-molded, quenched PEN film that was used for the kinetic studies exhibited a glass transition at 118°C, a broad cold-crystallization exotherm starting at 180°C, and a relatively sharp melting peak at 260°C (Fig. 1). An absolute enthalpy of about 28 J g^{-1} for both cold crystallization and melting indicated that the quenched PEN film was amorphous. Upon cooling, a crystallization exotherm was observed at 205°C.

Typical isothermal DSC curves in Figure 2 show the exothermic heat flow as a function of time for the cold crystallization of PEN and melt crystallization after melting at 290°C. The relative crystallinity X_t, defined as the ratio of crystallinity at time t to crystallinity when time approached infinity, is given as

$$X_t = \frac{\int_0^t (dH/dt)dt}{\int_0^\infty (dH/dt)dt} = \frac{\Delta H_t}{\Delta H_\infty} \quad (1)$$

where dH/dt is the rate of heat evolution; ΔH_t, the total heat evolved at time t; and ΔH_∞, the total heat evolved as time approaches infinity.

Plots of the relative crystallinity as a function of time showed the sigmoidal shape typical of isothermal polymer crystallization (Fig. 3). From the isotherms, the half-time of crystallization $t_{1/2}$, defined as the time required to reach $X_t = 0.5$, was determined (Table I).

Typically, $t_{1/2}$ represents the overall crystallization rate and is governed by the rates of nucleation and crystal growth. The combined effect of the two rates produces a maximum in the crystallization rate at a temperature between the melting point and the glass transition temperature and gives rise to the so-called bell curve of isothermal crystallization. Figure 4 illustrates the variation of $t_{1/2}$ with the crystallization temperature for PEN. The crystallization rate is about the same for cold and melt crystallization and passes through a broad maximum (minimum in $t_{1/2}$) at about 200–220°C.[16,17,22] The higher rate of melt crystallization compared to cold crystallization at 180°C is attributed to formation of additional nuclei during cooling of the melt (nominally at 100°C min^{-1}) from 290°C to the crystallization temperature.

Following the classic Avrami equation,

$$1 - X_t = \exp(-kt^n) \quad (2)$$

where k is the crystallization rate constant and n is the Avrami exponent describing the crystal growth geometry and nucleation mechanism, the data in Figure 3 were plotted according to

$$\ln[-\ln(1 - X_t)] = n\ln t + \ln k \quad (3)$$

to obtain the Avrami parameters n and k.[23] Typically, Avrami plots exhibit an initial linear region with deviation at longer times as the growth rate decreases because of crystal impingement.

Most of the Avrami plots for cold and melt crystallization of PEN did not show a distinct deviation from linearity in the later stages of crystallization (Fig. 5). However, for consistency, the Avrami exponent n and the rate constant k were always calculated from the linear portion of primary crystallization between $X_t = 0.01$ and $X_t = 0.50$. The results are summarized in Table I. In most cases, the exponent n was close to 3, corresponding to spherulitic growth with athermal nucleation, that is, all the crystals started to grow at the same time. However, there were two exceptions: One was melt crystallization at 180°C ($n = 2.4$). As suggested above, the reason might lie in the formation of nuclei during cooling to the crystallization temperature. The reason for the low Avrami exponent for melt crystallization at 230°C ($n = 2.3$) is not clear. However, it should be noted that other investigators reported $n = 2.3$ for the crystallization of PEN from the melt at 230–260°C after melting at 280 or 320°C.[17] Avrami exponents between 2.5 and 3 have been reported for cold crystallization of PEN.[17,24]

Isothermal crystallization of PEN at 220°C from higher melt temperatures, 300 and 310°C, decreased the overall rate of crystallization [Fig. 6(a)] and re-

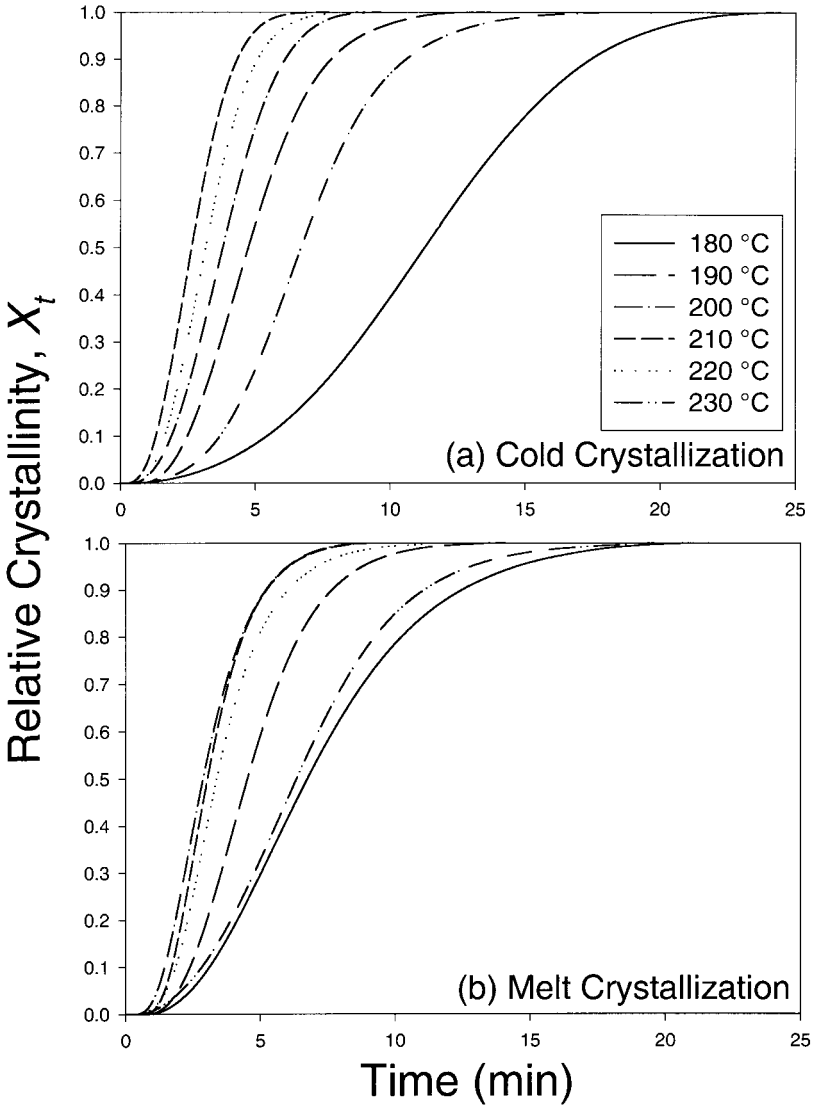

Figure 3 Relative crystallinity of PEN as a function of time obtained from DSC traces in Figure 2 (a) cold-crystallized at the temperature indicated and (b) melted at 290°C and crystallized at the temperature indicated.

TABLE I
Isothermal Crystallization Kinetics Parameters for PEN

Crystallization mode	Crystallization temperature (°C)	$t_{1/2}$ (min)	n	k (min^{-n})	ΔH_∞ (J g^{-1})	t_∞ (min)
Cold crystallization	230	6.7	3.2	0.0016	38	17.9
	220	3.2	2.9	0.026	35	9.1
	210	2.7	2.7	0.051	36	7.5
	200	3.8	2.7	0.019	36	9.5
	190	4.8	2.9	0.0079	36	12.7
	180	11.3	2.6	0.0013	35	24.1
Melt crystallization (from 290 °C)	230	6.4	2.3	0.0092	33	18.4
	220	3.4	3.1	0.016	38	12.6
	210	3.1	3.2	0.020	34	9.1
	200	2.9	2.7	0.038	32	8.8
	190	4.5	2.9	0.0086	30	13.9
	180	6.8	2.4	0.0071	29	21.6
Melt crystallization (from 300°C)	220	4.4	2.7	0.014	40	15.4
Melt crystallization (from 310°C)	220	5.8	2.1	0.019	39	18.6

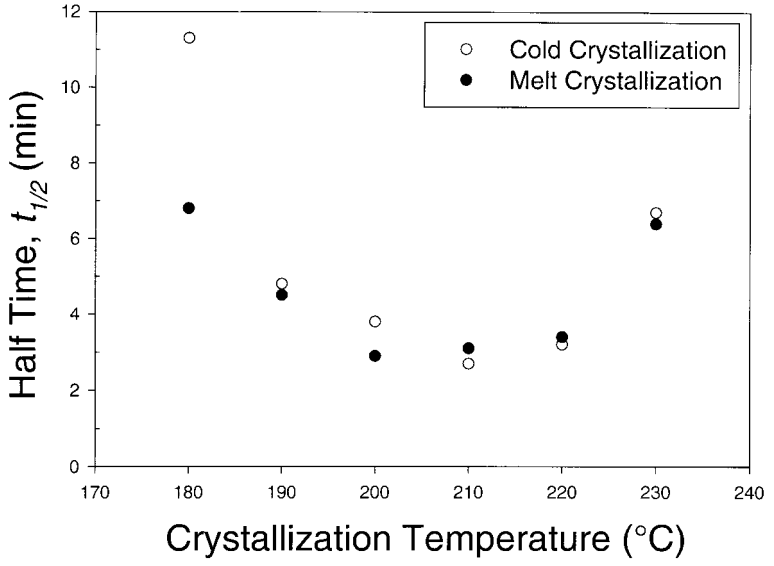

Figure 4 Half-time for crystallization of PEN.

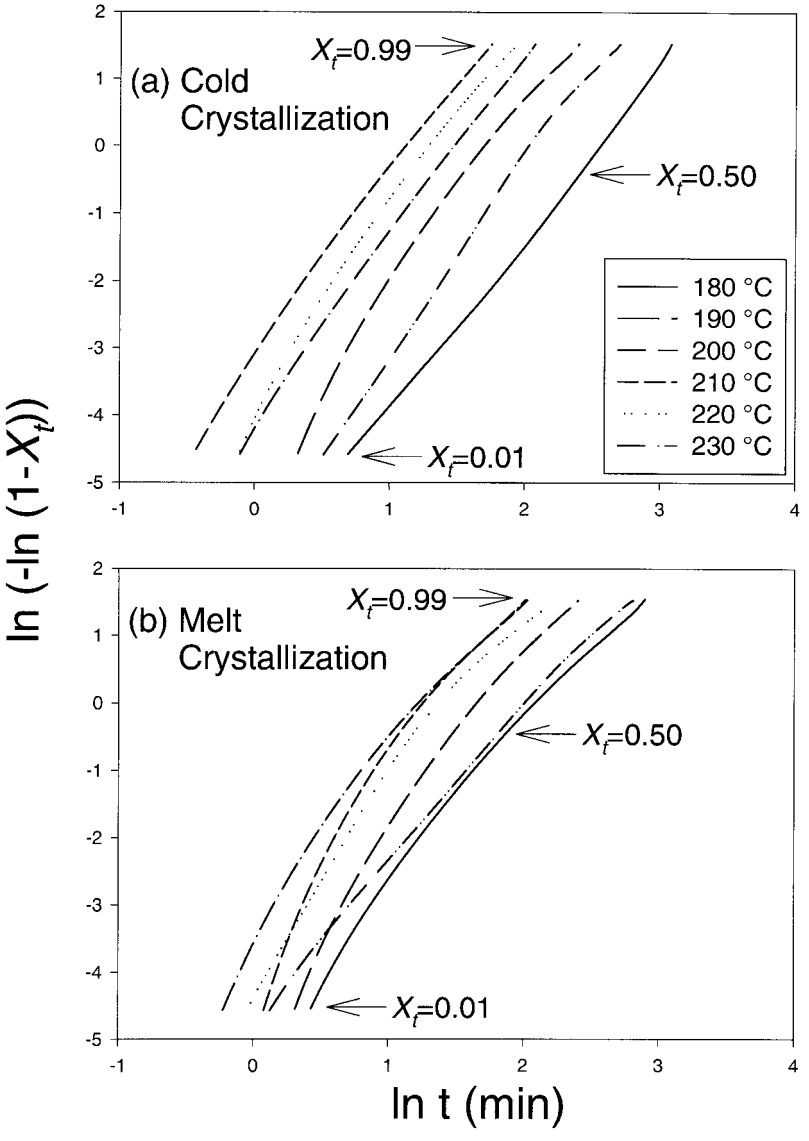

Figure 5 Relative crystallinity of PEN from Figure 3 plotted according to the Avrami relationship: (a) cold-crystallized at the temperature indicated; (b) melted at 290°C and crystallized at the temperature indicated.

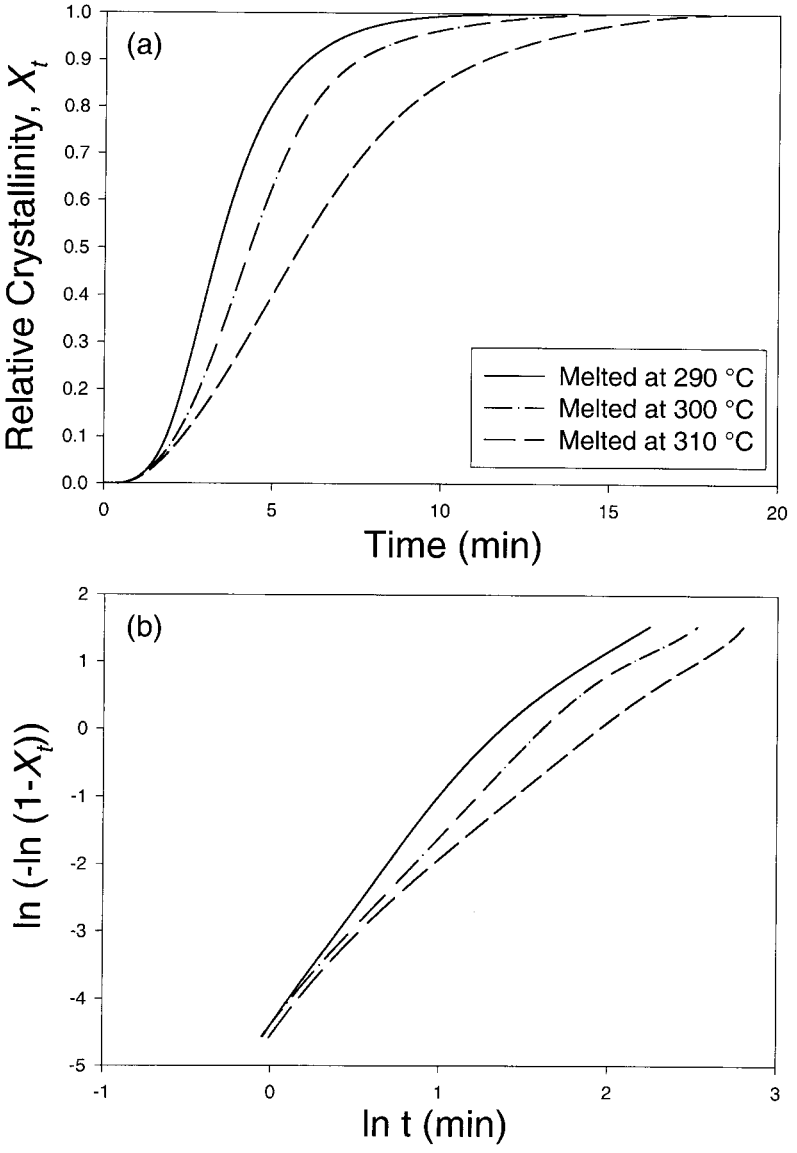

Figure 6 Crystallization of PEN at 220°C after melting at the temperature indicated: (a) relative crystallinity; (b) plotted according to the Avrami relationship.

duced the Avrami exponent from 3.1 to 2.1 [Fig. 6(b)]. This is a general phenomenon and is attributed to a gradual reduction in the number of self-nuclei as the temperature is increased above the melting point.[25,26] Although it is not unusual for the melt temperature to affect the Avrami exponent,[27,28] the previous study of PEN crystallization found no effect on n with an increasing melt temperature from 290 to 310°C.[17]

Crystal structure and morphology of isothermally crystallized of PEN

Two crystal forms have been described for PEN, α and β, depending on the thermal history.[16,29,30] The α crystal form shows three strong reflections at 2θ values of 15.6°, 23.3°, and 27.0°, corresponding to the (010), (100), and (−110) diffraction planes, and the β crystal form shows strong reflections at 2θ of 16.4°, 18.6°, and 25.5°, corresponding to the (−1–11), (020), and (2–42) diffraction planes.[16,31,32] These reflections were used to identify the crystal form of isothermally crystallized PEN from the WAXS patterns in Figure 7. Cold-crystallized PEN took, primarily, the α-form. Melt crystallization also produced the α-form after melting at 310°C and crystallizing at 220°C. However, melt crystallization after melting at a lower temperature of 290°C produced more complex results. Crystallization at 180°C produced only the α-form, whereas crystallization at higher temperatures of 220 and 230°C resulted in a mixture of α- and β-modifications. Other researchers reported mixed α- and β-modifications from the isothermal crystallization of PEN and postulated the existence of two types of nuclei as the source

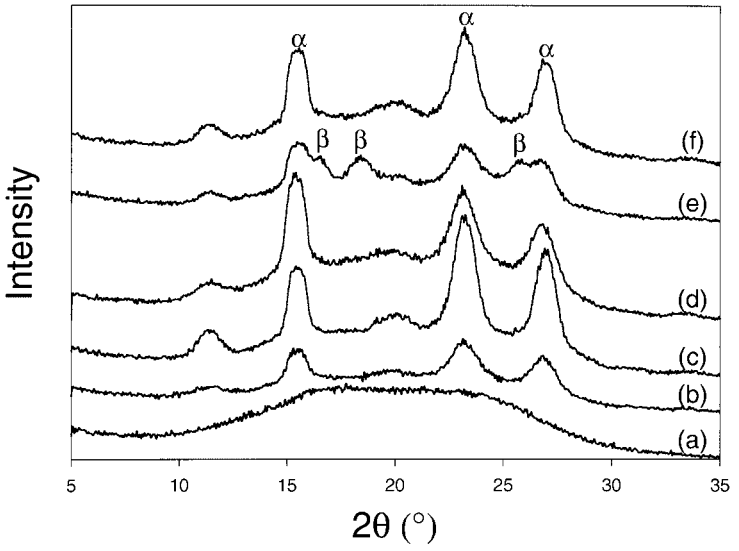

Figure 7 WAXS patterns of PEN: (a) quenched; (b) cold-crystallized at 180°C; (c) cold-crystallized at 230°C; (d) melted at 290°C and crystallized at 180°C; (e) melted at 290°C and crystallized at 220°C; (f) melted at 310°C and crystallized at 220°C.

of two crystal modifications with different crystallization rates.[16]

Three crystallization conditions were chosen on the basis of the WAXS results for examining the developing morphology: cold crystallization at 180°C (α-form), melt crystallization at 220°C after melting at 310°C (α-form), and melt crystallization at 220°C after melting at 290°C (α-form and β-form). At various time points, crystallization was arrested and the morphology was examined by AFM.

Before crystallization, the amorphous PEN film displayed a granular texture in the 3–μm AFM phase image [Fig. 8(a)]. The granules were in the 20–30-nm-size scale. The spherulitic morphology that developed during isothermal crystallization was revealed best by 25-μm AFM height images. After a relatively short crystallization time of 7.3 min (X_t = 0.25), individual spherulites with almost a perfect spherical shape were embedded in an amorphous matrix [Fig. 8(b)]. In higher-resolution phase images, the nonspherulitic regions exhibited the same granular texture as that of the quenched film. The spherulite diameter was in the range of 2.2–4.5 μm. After 10 min (X_t = 0.50), the spherulite size increased to 5.1–5.7 μm [Fig. 8(c)]. Some of the spherulites impinged; the nonimpinged spherulites retained the spherical shape. After 30 min (X_t = 1.00), the space-filling spherulites had grown to 7.0–8.1 μm [Fig. 8(d)].

The spherulites exhibited a regular banding pattern with spacing of about 0.63 μm. Persistence of a constant band spacing during isothermal spherulite growth conforms with the general observation that the banding period is determined primarily by the crystallization temperature.[33] A 3-μm-height image [Fig. 8(e)] and the corresponding phase image [Fig. 8(f)], taken from a spherulite arm, clearly showed the regular banding pattern produced by radial twisting of densely packed lamellae. In the height image, bright rings consisted of lamellae lying flat, whereas dark rings were composed of lamellae standing on edge. Lamellar thickness measured from the phase image was about 22–27 nm.

The AFM images in Figure 9 show PEN that was melted at 310°C and isothermally crystallized at 220°C. After crystallization for 3.3 min (X_t = 0.25), regular spherulites with a spherical shape and distinct boundaries were observed [Fig. 9(a)]. After crystallization for 60 min (X_t = 1.00), the morphology consisted of space-filling spherulites of about 28–32 μm [Fig. 9(b)]. The distinctive 2.7-μm banding pattern was much larger than was the band spacing of PEN cold-crystallized at 180°C (spacing of 0.63 μm) in accordance with the general observation that the band spacing increases with the crystallization temperature.[33–37]

The AFM images in Figure 10 show PEN that was melted at a lower temperature of 290°C and isothermally crystallized at 220°C. After a short crystallization time of 2.7 min (X_t = 0.30), the morphology consisted of irregularly shaped structures embedded in an amorphous matrix [Fig. 10(a)]. In a 3-μm phase image, the amorphous background exhibited a granular texture with an average size of the granules of about 15–20 nm [Fig. 10(b)]. The texture closely resembled that of the quenched film [cf. Fig. 8(a)]. The similarity indicated that the cooling rate of the isothermally crystallized specimens (nominally 300°C min^{-1} in the DSC) was fast enough to quench uncrystallized PEN to the amorphous state.

The irregular crystalline structures formed in the initial stages of crystallization [Fig. 10(a)] resembled

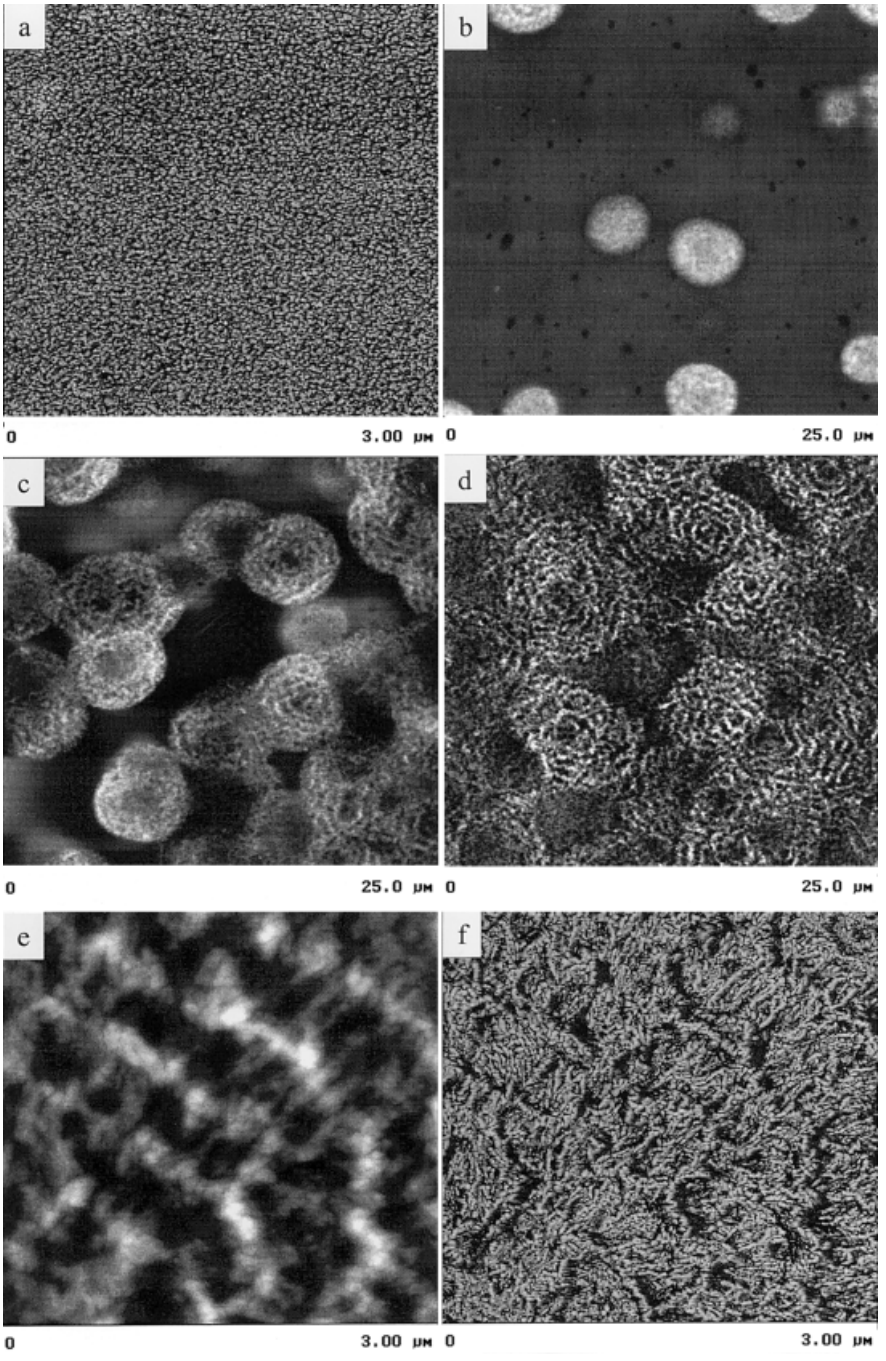

Figure 8 AFM images of PEN cold-crystallized at 180°C: (a) higher-resolution phase image of the amorphous film; (b) height image after crystallization for 7.3 min (X_t = 0.25); (c) height image after crystallization for 10 min (X_t = 0.50); (d) height image after crystallization for 30 min (X_t = 1.00); (e) higher-resolution height image from a spherulite arm in (d); (f) the corresponding phase image.

the hedrites described previously.[17] Crystallization for 3.8 min (X_t = 0.60) produced a mixed morphology with features of hedrites and spherulites [Fig. 10(c)]. Very likely, the mixed morphology was related to the coexistence of two crystalline forms. After 30 min (X_t = 1.00), the spherulites were space-filling [Fig. 10(d)]. The banding pattern was well developed with a spacing of 2.7 μm. The spherulites were much smaller than were those crystallized at 220°C after melting at 310°C, which was consistent with a higher nucleation density and a higher overall rate of crystallization. However, the band spacing was the same.

Isothermal crystallization kinetics of PETBB55

The heating thermogram of the compression-molded, quenched film that was used for the kinetic studies

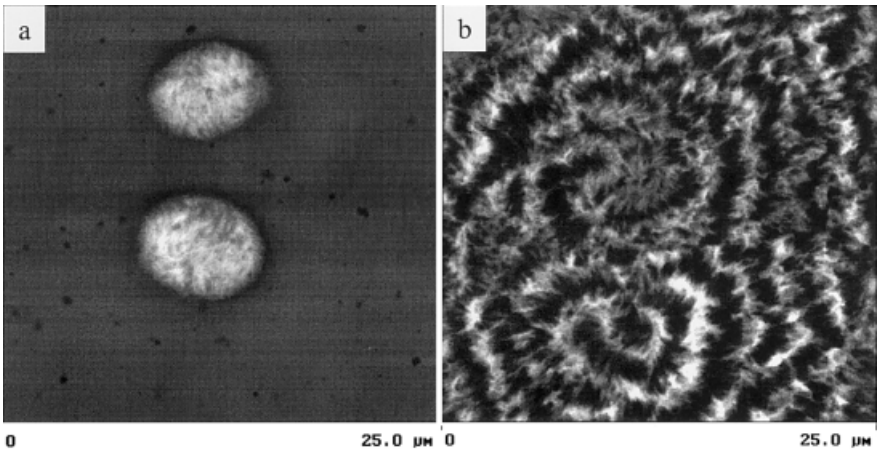

Figure 9 AFM height images of PEN melted at 310°C and crystallized at 220°C: (a) crystallized 5.3 min (X_t = 0.25); (b) crystallized 60 min (X_t = 1.00).

exhibited a glass transition at 104°C, a sharp cold-crystallization exotherm at 118°C, and a broad melting peak at 180–270°C (Fig. 11). Indeed, the breadth of the melting endotherm made the determination of the melting enthalpy difficult. However, similar enthalpies of cold crystallization and melting and the absence of crystalline reflections in the WAXD indicated that the quenched film used in the kinetic studies was essentially amorphous. The enthalpies associated with the cold crystallization and melting peaks were about

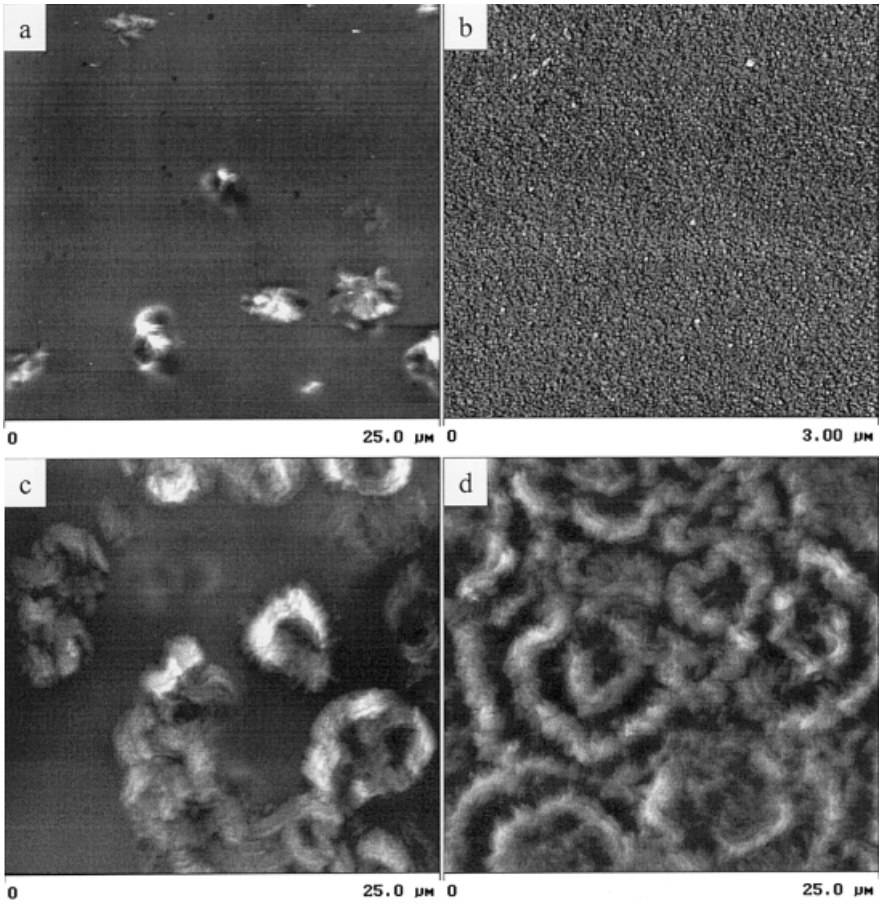

Figure 10 AFM images of PEN melted at 290°C and crystallized at 220°C: (a) height image after crystallization for 2.7 min (X_t = 0.30); (b) higher-resolution phase image of an uncrystallized region of (a); (c) height image after crystallization for 3.8 min (X_t = 0.60); (d) height image after crystallization for 30 min (X_t = 1.00).

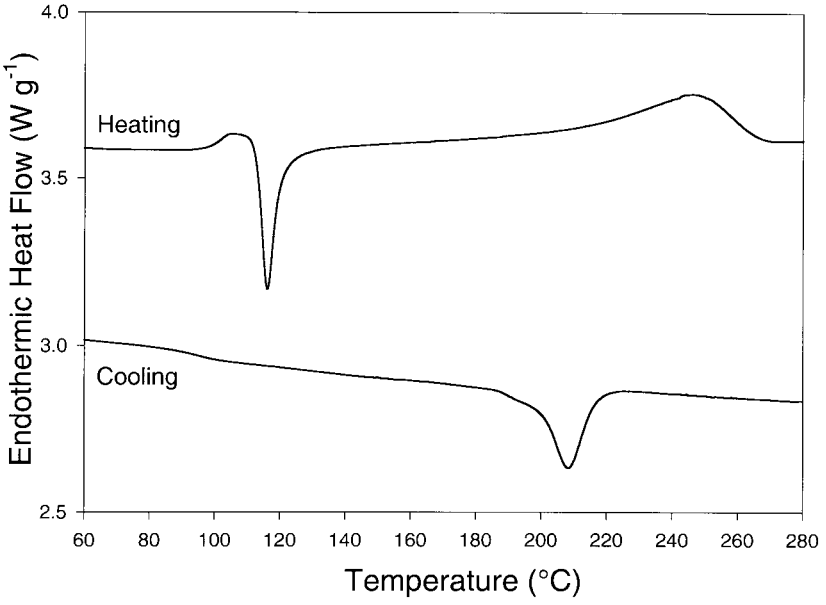

Figure 11 Heating and cooling thermograms of quenched PETBB55 film obtained with a scanning rate of 10°C min^{-1}.

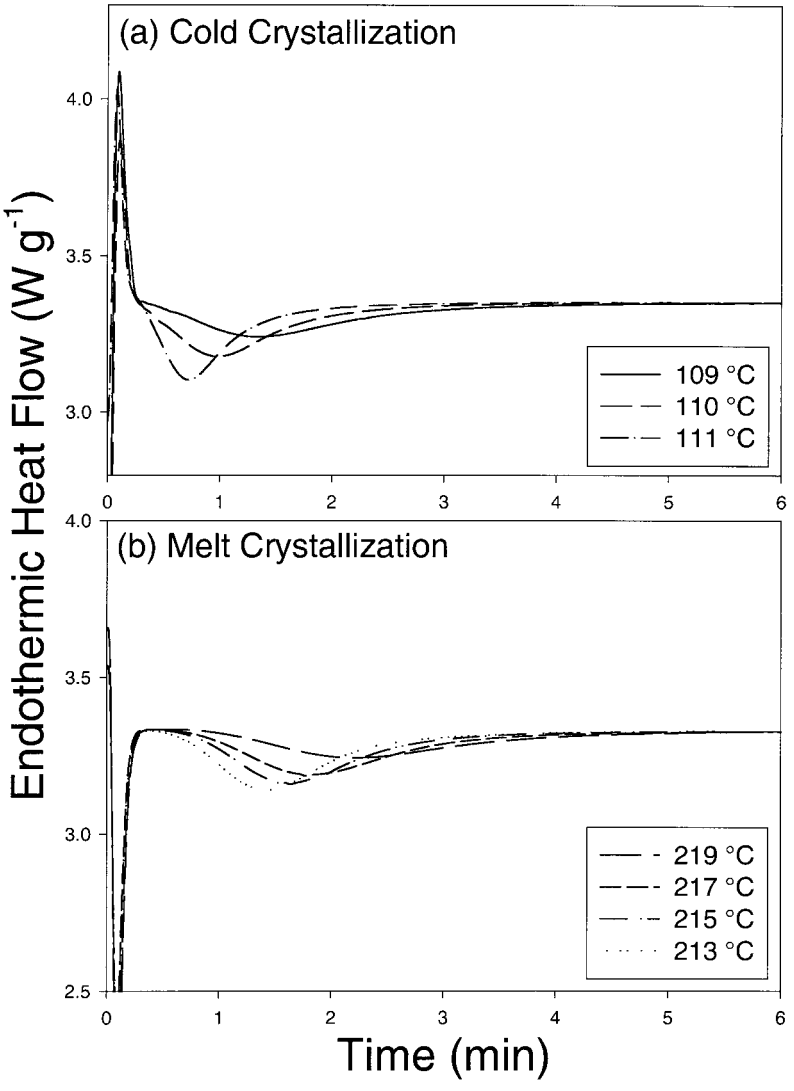

Figure 12 Isothermal DSC traces for crystallization of PETBB55: (a) cold-crystallized at the temperature indicated; (b) melted at 290°C and crystallized at the temperature indicated.

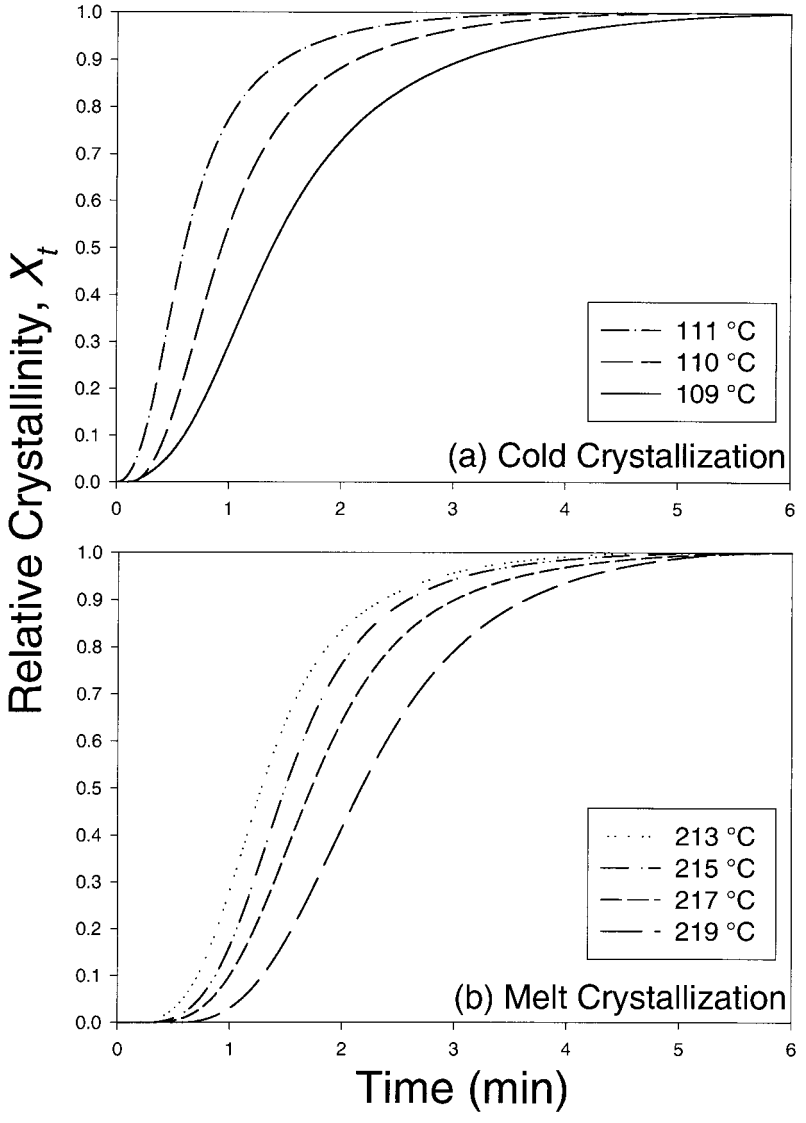

Figure 13 Relative crystallinity of PETBB55 as a function of time obtained from DSC traces in Figure 12: (a) cold-crystallized at the temperature indicated; (b) melted at 290°C and crystallized at the temperature indicated.

26 J g^{-1}. Upon cooling, a crystallization exotherm was observed at 208°C.

Comparison of the thermograms indicated that PETBB55 (Fig. 11) crystallized much more rapidly than did PEN (Fig. 1). Faster cold crystallization of PETBB55 was evident in the lower temperatures of the cold-crystallization exotherm; indeed, cold crystallization immediately followed the onset of molecular mobility at the glass transition and the sharper crystallization exotherm. However, the breadth of the subsequent PETBB55 melting endotherm suggested that the crystals formed during cold crystallization were not as uniform as were the cold-crystallized PEN crystals. Faster crystallization of PETBB55 from the melt was evident in the smaller undercooling and sharper crystallization exotherm compared to PEN.

Because the crystallization of PETBB55 was much faster than was the crystallization of PEN, the range of crystallization temperatures for the kinetic study was limited to 109–111°C for cold crystallization and 213–219°C for melt crystallization. Typical isothermal DSC curves show the exothermic heat flow during crystallization of PETBB55 from the glass and the melt (Fig. 12). Plots of the relative crystallinity as a function of time had the typical sigmoidal shape (Fig. 13). The half-time of crystallization $t_{1/2}$ is given in Table II. The fast crystallization of PETBB55 was clearly evident in the temperature dependence of $t_{1/2}$ (Fig. 14). On either side of the bell curve, the $t_{1/2}$ of PETBB55 decreased rapidly and was less than 1 min at temperatures well removed from the anticipated peak in the crystallization rate, whereas the entire temperature range was accessible for measuring the crystallization kinetics of PEN, and at the temperature of the fastest crystallization, $t_{1/2}$ was about 3 min.

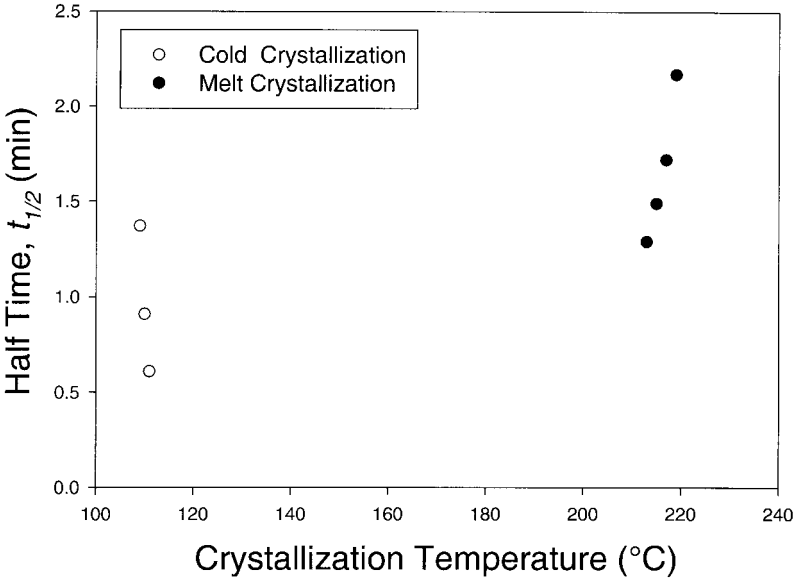

Figure 14 Half-time for crystallization of PETBB55.

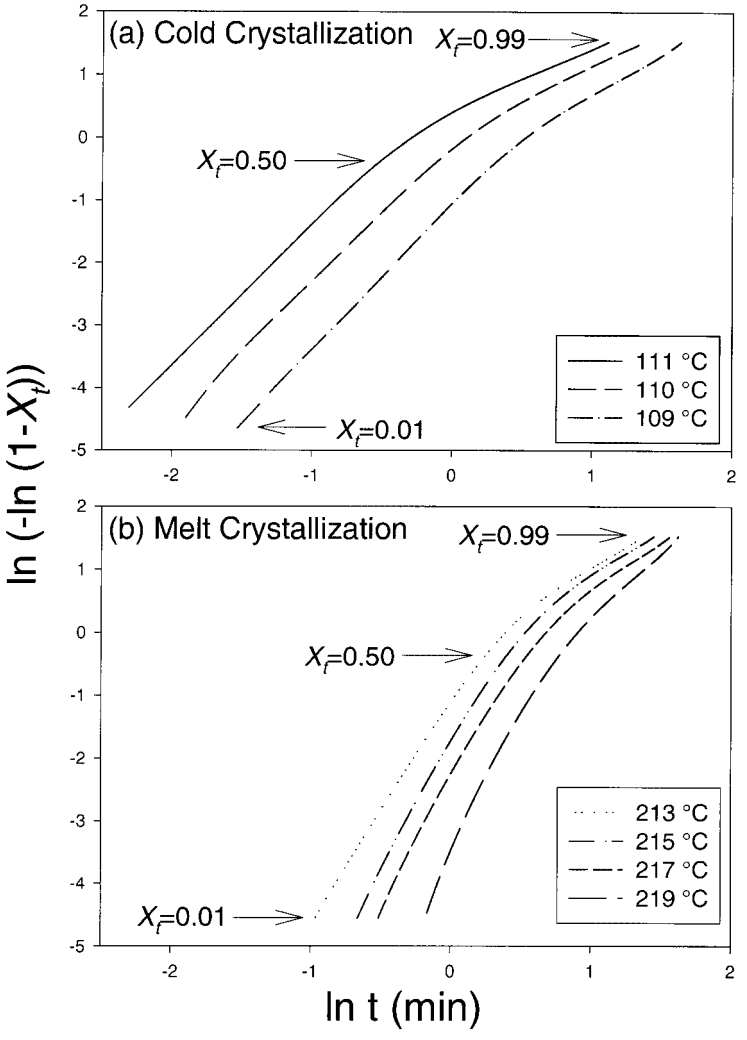

Figure 15 Relative crystallinity of PETBB55 from Figure 13 plotted according to the Avrami relationship: (a) cold-crystallized at the temperature indicated; (b) melted at 290°C and crystallized at the temperature indicated.

TABLE II
Isothermal Crystallization Kinetics Parameters for PETBB55

Crystallization mode	Temperature (°C)	$t_{1/2}$ (min)	n	k (min^{-n})	ΔH_∞ ($J\ g^{-1}$)	t_∞ (min)
Cold crystallization	109	1.4	2.3	0.34	11	6.3
	110	0.9	2.1	0.82	12	5.0
	111	0.6	2.2	1.8	12	4.5
Melt crystallization	219	2.2	3.5	0.056	11	6.1
	217	1.7	3.4	0.12	13	6.2
	215	1.5	3.4	0.19	14	5.6
	213	1.3	3.3	0.32	14	5.0

The difference in the crystallization rate appeared in the measured crystallization enthalpies. For PEN, the isothermal heat of melting (Table I) was equal to or larger than the 28 J g^{-1} for crystallization and melting in the heating thermogram (Fig. 1); however, the isothermal heat of melting of PETBB55 (Table II) was about one-half the 26 J g^{-1} in the heating thermogram (Fig. 11). Apparently, even at temperatures far from the maximum rate, crystallization of PETBB55 was fast enough that crystallization during the 0.3-min equilibration time was significant.

Avrami plots for cold- and melt-crystallized PETBB55 are shown in Figure 15. In contrast to the Avrami plots of PEN, those of PETBB55 showed a distinct bend at about $X_t = 0.65$. For consistency, the Avrami exponent n and the rate constant k were always calculated from the linear portion of primary crystallization between $X_t = 0.01$ and $X_t = 0.50$. The melt crystallization of PETBB55 had an Avrami exponent of about 3, which is usually interpreted as indicating 3-dimensional spherulitic growth; however, cold crystallization had an n value of about 2 (Table II).

Crystal structure and morphology of isothermally crystallized PETBB55

The WAXS pattern of the quenched PETBB55 film used in the kinetic studies exhibited a broad amorphous peak with no evidence of sharp crystalline reflections. After cold crystallization at 155°C or melt crystallization at 215°C, the pattern contained four crystalline diffraction peaks superimposed on the broad amorphous peak (Fig. 16). In PETBB55 cold-crystallized at a lower temperature (110°C), the crystalline reflections were broader and overlapped and the amorphous peak was more evident.

The crystal structure of PETBB55 has not been reported. The homopolymer, PEBB, crystallizes in a triclinic unit cell ($a = 5.75$, $b = 3.82$, $c = 14.62$ Å; $\alpha = 90.1$, $\beta = 90.3$, $\gamma = 78.1°$) with 2θ values of 15.7°, 16.9°, 24.1°, and 26.2° for reflections from the (100), (−101), (010), and (110) planes.[38] Diffraction peaks in the WAXS pattern of PETBB55 corresponded to the 2θ values expected for PEBB, except that the (110) reflection shifts slightly from 26.2° to 25.9°. Although the diffraction pattern of the PET crystal differs considerably, the chain configuration in the PET crystal resembles that of PEBB in many respects.[38] It appears that terephthalate units readily cocrystallize with bibenzoate in a PEBB-like crystal. This study is not the first to demonstrate the apparent ease with which the PEBB crystal accommodates comonomer units. Other researchers have shown that poly(ethylene napthalate-*co*-bibenzoate) with a higher naphthalate content readily crystallizes in a PEBB-like crystal structure with uniform comonomer inclusion.[14]

Morphologically, the quenched amorphous PETBB55 film displayed a granular texture in the 3-μm AFM phase image [Fig. 17(a)]. The granular texture was retained when crystallization was arrested at various times during cold crystallization at 111°C. The granular size might have increased slightly from 15–20 nm to 23–36 nm ($X_t = 1.00$) and the granular boundaries might have become sharper after cold crystallization [Fig. 17(b)]. However, it was noteworthy that the very substantial level of crystallinity achieved by cold crystallization produced no morphological features other than the granular texture. Indeed, PETBB55 cold-crys-

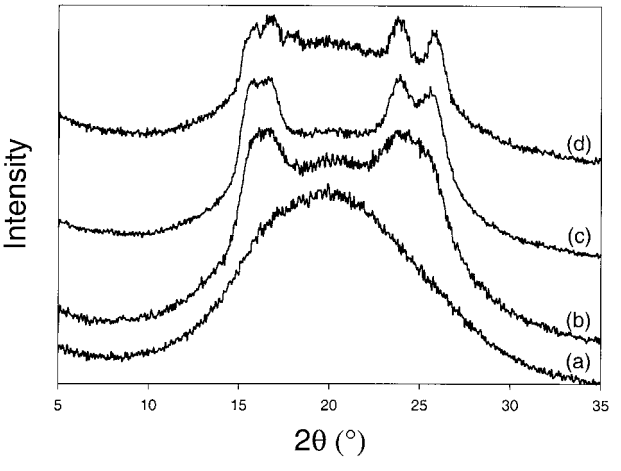

Figure 16 WAXS patterns of PETBB55: (a) quenched; (b) cold-crystallized at 110°C; (c) cold-crystallized at 155°C; (d) melt-crystallized at 215°C.

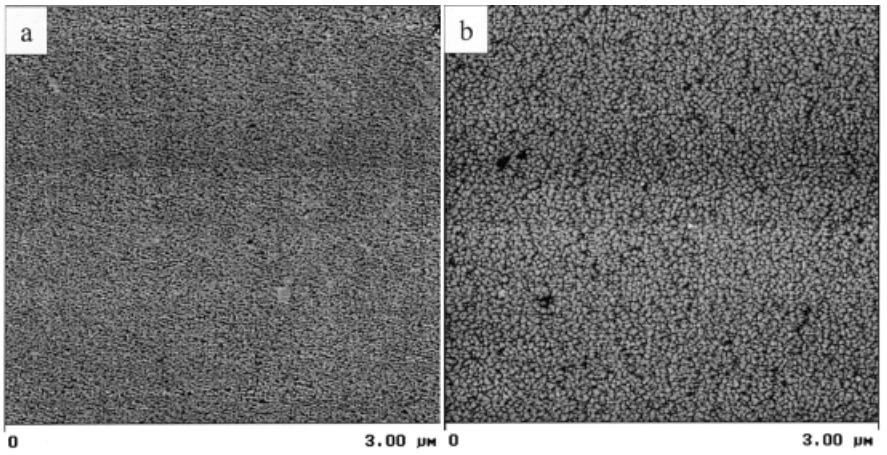

Figure 17 AFM phase images of PETBB55: (a) the quenched film; (b) cold-crystallized at 111°C for 30 min (X_t = 1.00).

tallized at a higher temperature of 155°C also retained the granular texture despite the high degree of crystalline order revealed by the WAXS pattern (see Fig. 16).

Crystallization of PETBB55 from the melt produced the AFM images in Figure 18. In consideration of the very rapid crystallization of PETBB55, a specimen in the melt at 290°C was quenched in the DSC at the rate used to arrest crystallization of partially crystallized specimens, nominally 300°C min^{-1}. This produced the coarse texture in Figure 18(a). A higher-resolution phase image showed numerous short irregular lamellar crystals [Fig. 18(b)]. The subsequent thermogram confirmed that the DSC-quenched PETBB55 was fully crystallized by showing a melting peak with an enthalpy of 26 J g^{-1} but no cold-crystallization exotherm. This contrasted with the thermogram of the cold water-quenched PETBB55 film used for cold crystallization (Fig. 11). The results indicated that even quenching at a nominal rate of 300°C min^{-1} was not fast enough to prevent complete crystallization of PETBB55. Therefore, it was assumed that the quenching process used to arrest isothermal crystallization would crystallize any uncrystallized polymer. Textural differences were used to differentiate isothermal crystallization from crystallization during quenching.

The 25-μm AFM image of PETBB55 that was isothermally crystallized at 213°C for 0.7 min (X_t = 0.10) contained spherulites about 7–9 μm in diameter with irregular open boundaries [Fig. 18(c)]. A higher-resolution image showed that the isothermally crystallized spherulites initially were sheaflike and consisted of loosely packed, long thin lamellae about 14 nm thick [Fig. 18(d)]. The surrounding nonspherulitic regions had a lamellar texture like that of the quenched melt in Figure 18(b). After crystallization for 10 min (X_t = 1.00), space-filling spherulites were about 10–12 μm in diameter [Fig. 18(e)]. As the crystallization time increased, lamellae in the spherulite arms became denser due to secondary crystallization and the thickness increased to 32–41 nm [Fig. 18(f)].

Comparison of PEN and PETBB55 crystallization

Crystallization of PEN is conventional in many respects. Crystallization from the melt and from the glassy state is slow enough that the kinetics is accessible by the standard thermal analysis method over the entire temperature range between the glass transition and melting. Crystallization from the melt and from the glass quenched from the same melt temperature exhibits a common relationship between the crystallization rate and the temperature. Also, the Avrami coefficient in both cases is close to 3 for heterogeneous nucleation with 3-dimensional crystal growth.[23] Correspondence between melt and cold crystallization indicates that rapid quenching retains existing nuclei in the melt while preventing formation of additional nuclei during cooling.

The interesting question is twofold: Why does PETBB55, a copolymer, crystallize much faster than does PEN, and why does PETBB55 crystallize from the melt in the conventional way for polyesters, that is, spherulitic growth with an Avrami coefficient of about 3, whereas it crystallizes from the glass in a substantially different way, that is, a granular crystalline morphology with an Avrami coefficient of 2. In view of the substantial level of crystallinity achieved by PETBB55, it is apparent that terephthalate units and bibenzoate units readily cocrystallize. Close resemblance between the WAXS patterns of the copolymer and the homopolymer PEBB indicates that terephthalate units are incorporated into the PEBB crystal structure. Copolymers of ethylene bibenzoate with a high naphthalate content similarly crystallize in a PEBB-like crystal structure. The PEBB crystal may accommodate terephthalate units in the same way that it accommodates

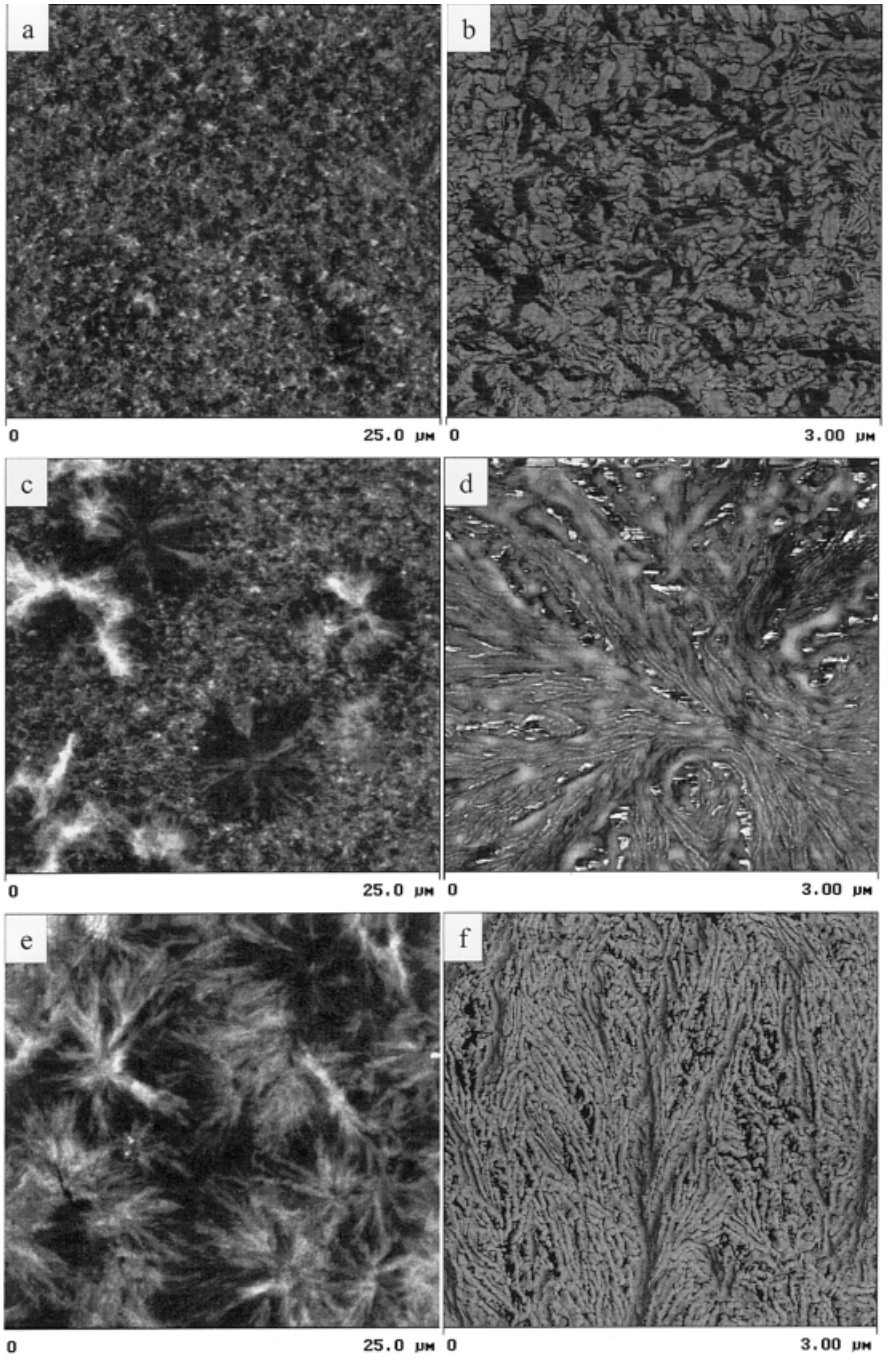

Figure 18 AFM images of PETBB55 melted at 290°C and crystallized at 213°C: (a,b) quenched in the DSC from 290°C; (c,d) crystallized for 0.7 min ($X_t = 0.10$); (e,f) crystallized for 10 min ($X_t = 1.00$). (a), (c), and (e) are height images; (b), (d), and (f) are phase images.

naphthalte units, namely, by uniformly incorporating comonomer-rich and bibenzoate-rich layers.[14]

It is interesting to recall that the homopolymer PEBB reportedly is liquid crystalline.[3] Even if terephthalate units disrupt the rodlike nature of PEBB chains enough to prevent formation of a recognizable mesophase, the copolymer may take a quasi-ordered state that is close to liquid crystalline. It seems reasonable that when the melt is cooled the quasi-ordered chains rapidly assemble into ordered crystalline arrays. The envisaged process resembles the concept of lamellar crystallization as a multistep process with an intermediate mesostructure that was recently proposed for crystallization of some polyolefins.[39] In this model, growth of the mesostructure is the slow step in lamellar crystallization. If the melt structure is already close to a mesophase, the slow step is virtually eliminated and crystallization becomes very rapid.

Very rapid crystallization of PETBB55 from the melt explains the unusual features of cold crystallization. Unlike quenching of the more slowly crystallizing PEN, PETBB55 cannot be quenched through the crystallization bell curve rapidly enough to prevent formation of many tiny crystalline nuclei. These nuclei are contained in the granules as ordered domains of parallel chains that may resemble fringed micellar crystals. When the temperature is increased above the glass transition, crystallization rapidly proceeds with further ordering of the chains in the granule. Two-dimensional growth of ordered domains from preexisting nuclei satisfies the Avrami condition for $n = 2$ (ref. 23) and conforms with previous reports of 2-dimensional crystallization from the liquid crystalline state.[40,41] Some increase in the granule size may occur at the expense of intergranule regions, and, indeed, the granules appear somewhat larger after cold crystallization; however, it should be noted that the granule size observed in the AFM is, to some extent, dependent on the etching conditions used for specimen preparation and tapping conditions used for imaging. As the structural units grow, some amount of aggregation is expected; however, nucleation is so dense that crystallization is essentially complete before this stage can proceed to a meaningful extent.

CONCLUSIONS

Crystallization of PETBB55 was shown to differ in important aspects from the crystallization of more conventional polyesters as exemplified in this study by PEN, whereas crystallization of PEN from the melt and from the glassy state was slow enough to permit characterization of the kinetics over the entire temperature range between the glass transition and the melting temperature; this was not the case for PETBB55. Except for a small temperature range on either side of the bell-shaped curve, crystallization of PETBB55 occurred too rapidly to obtain the kinetics by standard thermal analysis methods. Crystallization of PETBB55 from the melt produced a spherulitic morphology and the kinetics conformed to an Avrami exponent close to 3 for heterogeneous nucleation with 3-dimensional crystal growth. In contrast, the crystallized glass exhibited a granular morphology that was not markedly different in appearance from the granular texture of the quenched glass. Cold-crystallization kinetics in accordance with an Avrami exponent of 2 for heterogeneous nucleation with 2-dimensional crystal growth confirmed different dimensionalities of cold and melt crystallization. Following from the known liquid crystalline nature of the homopolymer PEBB, it was proposed that the copolymer assumed a quasi-ordered state that was close to liquid crystalline. Upon cooling, the chains rapidly assembled into a crystalline structure. As a consequence of rapid crystallization, quenching from the melt probably was not fast enough to prevent formation of additional nuclei. The nucleation density for crystallization from the glass was high enough that the growth of crystalline entities could not proceed beyond the initial stages.

This research was generously supported by KoSa and the National Science Foundation (Grants DMR 9975774 and DMR 9986467). Support from Modern Controls, Inc., for development of a facility for gas-transport studies at Case Western Reserve University, is gratefully acknowledged by the authors.

REFERENCES

1. Liu, R. Y. F.; Schiraldi, D. A.; Hiltner, A.; Baer, E. J Polym Sci Part B Polym Phys 2002, 40, 862.
2. Ma, H.; Hibbs, M.; Collard, D. M.; Kumar, S.; Schiraldi, D. A., submitted for publication in Macromolecules.
3. Krigbaum, W. R.; Asrar, J.; Toriumi, H.; Ciferri, A.; Preston, J. J Polym Sci Polym Lett Ed 1982, 20, 109–115.
4. Meurisse, P.; Noel, C.; Monnerie, L. Fayolle, B. Br Polym J 1981, 13, 55–63.
5. Krigbaum, W. R.; Watanabe, J. Polymer 1983, 24, 1299–1307.
6. Tokita, M.; Takahashi, T.; Hayashi, M.; Inomata, K.; Watanabe, J. Macromolecules 1996, 29, 1345–1348.
7. Watanabe, J.; Hayashi, M.; Nakata, T.; Niori, T.; Tokita, M. Prog Polym Sci 1997, 22, 1053–1087.
8. Jung, H.-T.; Hudson, S. D.; Lenz, R. W. Macromolecules 1998, 31, 637–643.
9. Schiraldi, D. A.; Occelli, M. L.; Gould, S. A. C. J Appl Polym Sci 2001, 82, 2616–2623.
10. Sherman, S. C.; Iretskii, A. V.; White, M. G.; Schiraldi, D. A. Chem Innov 2000, 30(7), 25–30.
11. Polyakova, A.; Liu, R. Y. F.; Schiraldi, D. A.; Hiltner, A.; Baer, E. J Polym Sci Part B Polym Phys 2001, 39, 1889–1899.
12. Sakaguchi, Y.; Okamoto, M.; Tanaka, I. Macromolecules 1995, 28, 6155–6160.
13. Asrar, J. J Polym Sci Part A Polym Chem 1999, 37, 3139–3146.
14. Wendling, J.; Gusev, A. A.; Suter, U. W.; Braam, A.; Leemans, L.; Meier, R. J.; Aerts, J.; van der Heuvel, J.; Hottenhuis, M. Macromolecules 1999, 32, 7866–7878.
15. Bicerano, J. JMS Rev Macromol Chem Phys 1998, 38, 391–479.
16. Buchner, S.; Wiswe, D.; Zachmann, H. G. Polymer 1989, 30, 480–488.
17. Lee, S. W.; Cakmak, M. J Macromol Sci Phys 1998, 37, 501–526.
18. Yu, L.; Shanks, R. A.; Stachurski, Z. H. Prog Polym Sci 1995, 20, 651.
19. Shabana, H. M.; Olley, R. H.; Bassett, D. C.; Zachmann, H. G. J Macromol Sci Phys B 1996, 35, 691–708.
20. Organ, S. J.; Barham, P. J. Polym Prepr 1988, 29, 602.
21. Hudson, S. D.; Vezie, D. L.; Thomas, E. L. Makromol Chem Rapid Commun 1990, 11, 651–662.
22. Gao, X.; Jin, M.; Bu, H. J Polym Sci Part B Polym Phys 2000, 38, 3285–3288.
23. Keller, A. In Polymers, Liquid Crystals and Low-Dimensional Solids; March, N.; Tosi, M., Eds.; Plenum: New York, London, 1984; Chapter 2.
24. Kajaks, J.; Flores, A.; Garcia Gutierrez, M. C.; Rueda, D. R.; Balta Calleja, F. J. Polymer 2000, 41, 7769–7772.
25. Frenkel, F. J Chem Phys 1939, 7, 538–547.
26. Zhang, Z.; Zeng, H. Makromol Chem 1992, 193, 1745–1752.
27. Hartly, F. D; Lord, F. W.; Morgan, L. B. Philos Trans R Soc Lond A 1954, 247, 23–34.
28. Rybnibar, F. Coll Czech Chem Commun 1960, 25, 1529–1539.

29. Mencik, Z. Chem Prum 1967, 17, 78–81.
30. Kimura, F.; Kimura, T.; Sukisaki, A.; Komatsu, M.; Sata, H.; Ito, E. J Polym Sci Part B Polym Phys 1997, 35, 2741–2747.
31. Vasanthan, N; Salem, D. R. Macromolecules 1999, 32, 6319–6325.
32. van der Heuvel, C. J. M.; Klop, E. A. Polymer 2000, 41, 4249–4266.
33. Keith, H. D.; Padden, F. J. Macromolecules 1996, 29, 7776–7786.
34. Schulze, K.; Kressler, J.; Kammer, H. W. Polymer 1993, 34, 3704–3709.
35. Wang, Z.; Wang, X.; Yu, D.; Jiang, B. Polymer 1997, 38, 5897–5901.
36. Abe, H.; Aoki, H.; Doi, Y. Macromol Symp 1998, 130, 81–89.
37. Ho, R. M.; Ke, K. Z.; Chen, M. Macromolecules 2000, 33, 7529–7537.
38. Li, X.; Brisse, F. Macromolecules 1994, 27, 2276–2282.
39. Strobl, G. Eur Phys J E 2000, 3, 165–183.
40. Pardey, R.; Zhang, A.; Gabori, P. A.; Harris, F. W.; Cheng, S. Z. D.; Adduci, J.; Facinelli, J. V.; Lenz, R. W. Macromolecules 1992, 25, 5060–5068.
41. Yandrasits, M. A.; Chen, J.; Arnold, F. E., Jr.; Cheng, S. Z. D.; Percec, V. Polym Adv Tech 1994, 5, 775–784.